Supporting Information

Label-Free Dynamic Detection of Single-Molecule Nucleophilic Substitution Reaction

Chunhui Gu,[1†] Chen Hu,[2†] Ying Wei,[3] Dongqing Lin,[3] Chuancheng Jia,[1] Mingzhi Li,[1] Dingkai Su,[1] Jianxin Guan,[1] Andong Xia,[4] Linghai Xie,[3] Abraham Nitzan,[5] Hong Guo, [2*] Xuefeng Guo [1*]

[1]Beijing National Laboratory for Molecular Sciences, State Key Laboratory for Structural Chemistry of Unstable and Stable Species, College of Chemistry and Molecular Engineering, Peking University, Beijing 100871, P. R. China;

[2]Center for the Physics of Materials and Department of Physics, McGill University, Montreal, Quebec H3A 2T8, Canada;

[3]Center for Molecular Systems and Organic Devices, Key Laboratory for Organic Electronics & Information Displays and Institute of Advanced Materials, Nanjing University of Posts & Telecommunications, Nanjing 210023, P. R. China;

[4]Institute of Chemistry, Chinese Academy of Sciences, Beijing 100190, P. R. China;

[5]Department of Chemistry, University of Pennsylvania, Philadelphia, PA 19104-6323, USA;

[†]These authors contributed equally to the work.

Table of Contents

1. Macroscopic Experiments.....**S3**

2. Molecular Synthesis.....**S14**

3. Device Characterization and Analysis.....**S18**

4 Characterization of Control Devices…….....**S20**

5. Theoretical Analysis and Physical Properties.....**S24**

6. Dynamic Analysis.....**S27**

7. Additional Experimental Results.....**S30**

8. References.....**S34**

1. Macroscopic Experiments

1.1 Product Characterization

9-phenyl-9-fluorenol (5.4 mg, 0.021 mmol) was dissolved into the mixture solution of anhydrous acetic acid (HAc) and trifluoroacetic acid (TFA) (1:1 vol/vol, 1 mL). After the powder was totally dissolved, a solution (20 μL) was taken out rapidly and dispersed into ethyl acetate (1 mL). Thin layer chromatography (TLC) was preliminarily applied to determine the product. The results showed that 9-phenyl-9-fluorenol had been completely consumed and the only product showed the same R_f value as 9-phenyl-9-fluorenyl acetate standard. GC-MS characterization was carried out with the combination of a 7890B GC system (Agilent Technologies Ltd.) and a 5977A MSD (Agilent Technologies Ltd.). Before GC injection, the ethyl acetate solution was dried with anhydrous potassium carbonate and filtered. The product showed a chromatographic peak at RT = 7.391 min with m/z = 300.1 (24.2) and 241.1 (100.0), which was similar to those of 9-phenyl-9-fluorenyl acetate standard: RT = 7.384 min, m/z = 300.1 (48.0) and 241.2 (100.0), but quite different from the reagent 9-phenyl-9-fluorenol: RT = 7.284 min, m/z = 258.1 (100.0) and 241.1 (31.7) (Figure S1). These results showed that a high-yield esterification occurs in the HAc/TFA solution. The MS spectrum also showed the disassociation process from 9-phenyl-9-fluorenyl acetate to the corresponding carbocation.

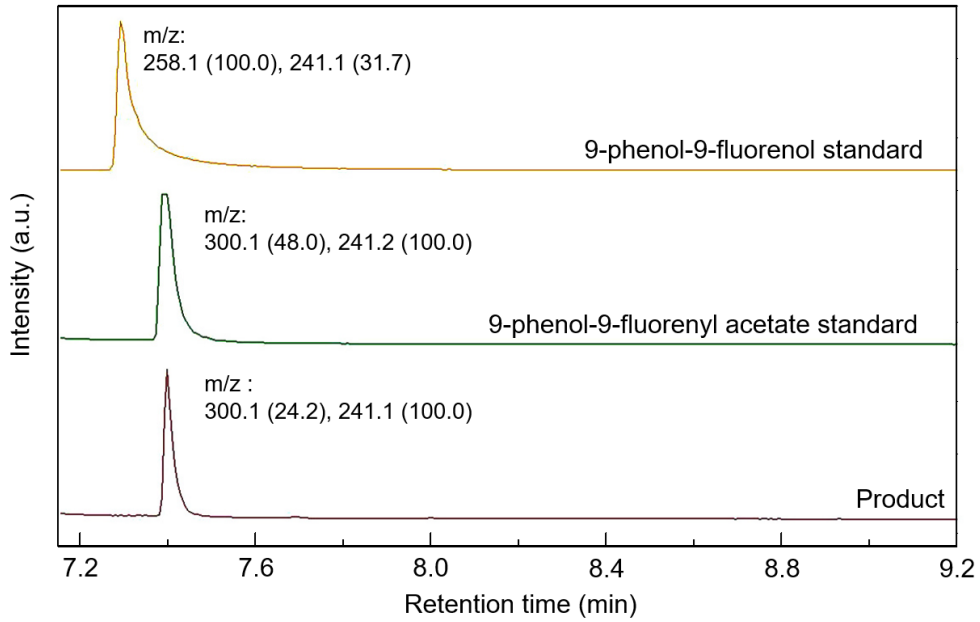

Figure S1. Chromatograms of 9-phenyl-9-fluorenol standard, 9-phenyl-9-fluorenyl acetate standard and the product (SIM mode, m/z = 241.1).

1.2 Thermodynamic Properties

We measured the combination constant (pK_{R+}) of 9-phenyl-9-fluorenyl cation and the generalized acid function (J_0) of the TFA/HAc solutions by an "indicator overlap" method described in Ref.[1]. J_0 is a generalized acidity function based on the ability of stabilizing carbocation initially defined in aqueous solution according to the following formula: [2]

$$J_0 = pK_{R+} + \lg\frac{[ROH]}{[R+]} \qquad \text{(Eq. 1)}$$

where [ROH]/[R^+] represents the ratio of two forms of the indicator: the alcohol/carbocation. K_{R+} is the combination constant of the carbocation, representing the equilibrium constant of the reaction:

$$R^+ + H_2O = ROH + H^+$$

$$K_{R+} = \frac{[ROH]}{[R+]}\frac{\alpha_{H^+}}{\alpha_{H_2O}} \qquad \text{(Eq. 2)}$$

Similarly, the concept of J_0 is valid in the non-aqueous solution. In a TFA/HAc solution, J_0 and K_{R+} are defined by replacing the solvent from water to acetic acid:

$$R^+ + HAc = RAc + H^+$$

$$J_0 = pK_{R+} + \lg\frac{[RAc]}{[R+]} \qquad \text{(Eq. 3)}$$

$$K_{R+} = \frac{[RAc]}{[R+]} \frac{\alpha_{H+}}{\alpha_{HAc}} \qquad \text{(Eq. 4)}$$

Six triarylcarbinols were applied as indicators. The absorption spectra were measured by an S4000 spectrophotometer (Hitachi Ltd.). For these compounds, the acetate forms (RAc) were achromatic in the vision region while the carbocation forms (R^+) absorbed at 430–490 nm (Table S3), which were characteristic. Figure S2 shows the absorption spectra of these indicators in carbocation forms.

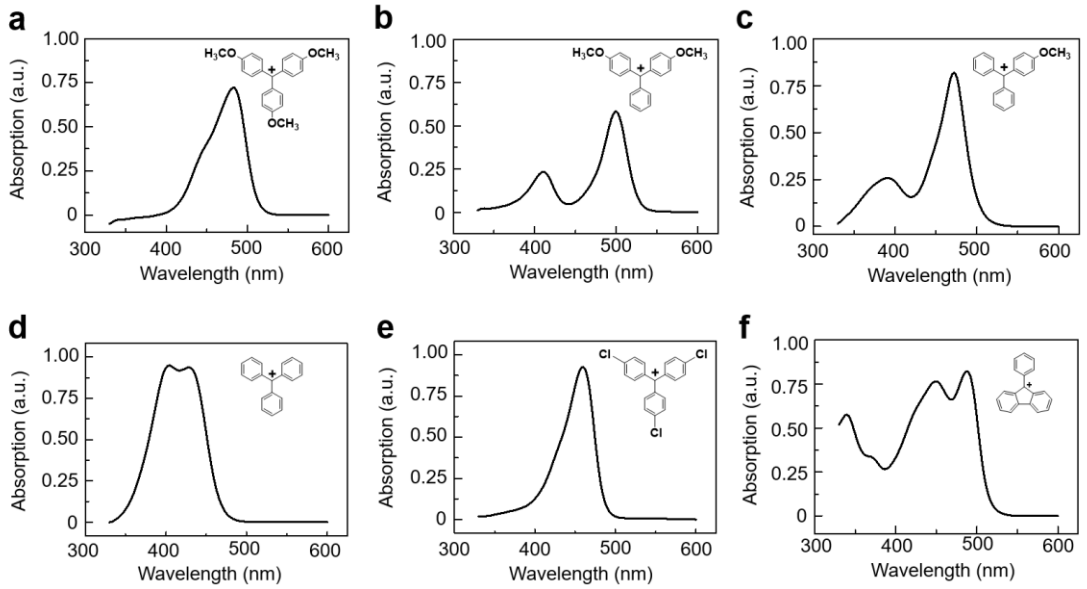

Figure S2. Absorption spectra: the carbocation forms of 4,4',4''-trimethoxytriphenylmethanol (a), 4,4'-dimethoxytriphenylmethanol (b), 4-methoxytriphenylmethanol (c), triphenylmethanol (d), 4,4',4''-trichlorotriphenylmethanol (e) and 9-phenyl-9-fluorenol (f).

We circumstantially measured the absorption of these indicators in HAc/water, TFA/HAc or TFA/sulfuric acid solutions (Figure S3). The proportion of carbocation can be quantified via the Lambert-Beer's law, which means, the absorbance of carbocation is in proportion with its concentration within the linear range (for 9-phenyl-9-fluorenyl cation, 0–50 μmol/L, Figure S4). The ratios [RAc]/[R^+] can be derived from the data in Figure S3 and their denary logarithm values are displayed in Table S2.

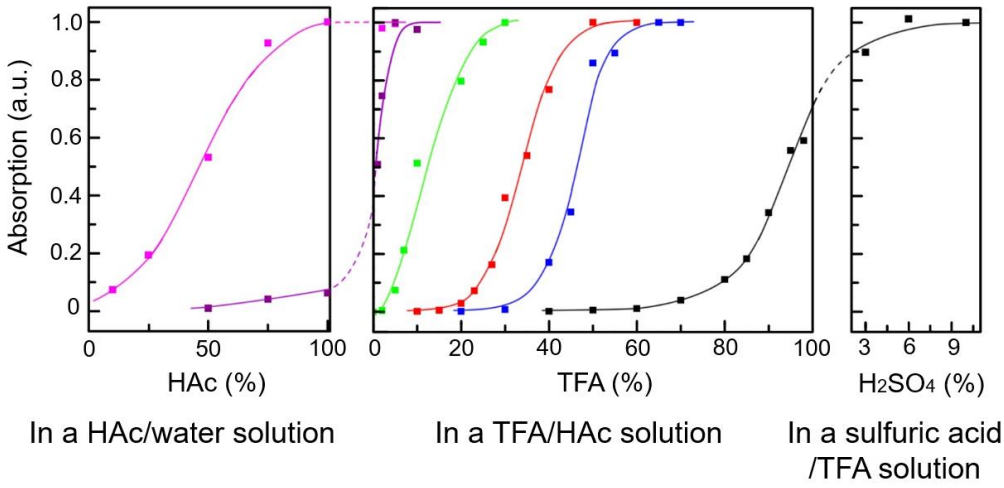

Figure S3. Normalized absorbance of six indicators in HAc/water, TFA/HAc and TFA/sulfuric acid solutions. Magenta, purple, green, red, blue and black dots represent the absorption of 4,4',4''-trimethoxytriphenylmethyl cation, 4,4'-dimethoxy triphenylmethyl cation, 4-methoxytriphenylmethy cation, triphenylmethyl cation, 4,4',4''-Trichlorotriphenylmethyl cation and 9-phenyl-9-fluorenyl cation, respectively. The solid line provides an eye guide.

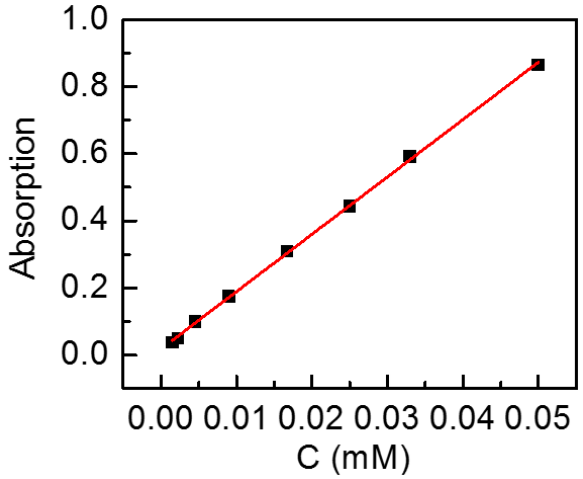

Figure S4. Linear range of the absorbance as a function of concentration for 9-phenyl-9-fluorenyl cation.

We measured the activity of proton (α_{H+}) in diluted HAc/water solutions via a pH meter (Table S1) and it was deemed that J_0 equals to the pH value in the diluted aqueous solution. Now that the acidity function J_0 was uniform in solution of the same composition, we could attain the J_0 values of high-acidity solutions, which were not suitable for ordinary pH measurements, through Equation 5. Furthermore, we could attain the combination constants K_{R+} of the indicators (Table S3).

$$J_0 = \mathrm{p}K_{\mathrm{R_1}+} + \lg\frac{[\mathrm{R_1Ac}]}{[\mathrm{R_1}+]} = \mathrm{p}K_{\mathrm{R_2}+} + \lg\frac{[\mathrm{R_2Ac}]}{[\mathrm{R_2}+]} \qquad \text{(Eq. 5)}$$

The derived J_0 values of TFA/HAc solutions (vol/vol) were listed in Table S2. The TFA proportion–J_0 plot was shown in Figure S5.

Table S1. pH values measured by a pH meter

Proportion		
H_2O%	HAc%	pH
95	5	2.06
90	10	1.87
83	17	1.65
75	25	1.51

Table S2. J_0 values measured by an "indicator overlapping" method

R = 4,4',4''-trimethoxytriphenylmethyl

Proportion			lg([RAc]/[R+])	J_0
H_2O%	HAc%	TFA%		
90	10	0	1.10	1.87
75	25	0	0.62	1.39
50	50	0	–0.06	0.72
25	75	0	–1.10	–0.33
0	100	0	N	N*
0	98	2	N	N
0	95	5	N	N

R = 4,4'-dimethoxytriphenylmethyl

Proportion			lg([RAc]/[R+])	J_0
H2O%	HAc%	TFA%		
50	50	0	2.02	0.32
25	75	0	1.37	–0.33
0	100	0	1.18	–0.52
0	99	1	–0.02	–1.72
0	98	2	–0.47	–2.17
0	95	5	N	N
0	90	10	N	N

R = 4-methoxytriphenylmethyl

Proportion		lg([RAc]/[R+])	J_0
HAc%	TFA%		
100	0	N	N
98	2	2.44	–2.17
95	5	1.10	–3.22
93	7	0.57	–3.83
90	10	–0.02	–4.51
80	20	–0.59	–4.71
75	25	–1.14	–5.38
70	30	N	N

R = triphenylmethyl cation

Proportion		lg([RAc]/[R+])	J_0
HAc%	TFA%		
90	10	N	N
85	15	N	N
80	20	1.53	–4.71
77	23	1.11	–5.13
73	27	0.71	–5.53
70	30	0.19	–6.05
65	35	–0.07	–6.31
60	40	–0.52	–6.76
50	50	N	N
40	60	N	N

R = 4,4’,4’’-Trichlorotriphenylmethyl cation

Proportion		lg([RAc]/[R+])	J_0
HAc%	TFA%		
80	20	N	N
70	30	N	N
60	40	0.69	–6.76
55	45	0.28	–7.17
50	50	–0.79	–8.24
45	55	–0.93	–8.38
35	65	N	N
30	70	N	N

R = 9-phenyl-9-fluorenyl

Proportion			lg([RAc]/[R+])	J_0
HAc%	TFA%	H2SO4%		
60	40	0	N	N
50	50	0	2.29	–8.24
40	60	0	1.97	–8.56
30	70	0	1.38	–9.14
20	80	0	0.90	–9.63
15	85	0	0.65	–9.88
10	90	0	0.28	–10.24
5	95	0	–0.10	–10.63
2	98	0	–0.16	–10.69
0	97	3	–0.99	–11.52
0	95	5	N	N
0	93	7	N	N

*N represents that the J_0 value is unable to be calculated

Table S3. Spectral properties and K_R of the indicators

Indicator	Maxinum absorption/nm	pK_{R+} in TFA/HAc	pK_{R+} in H_2SO_4/H_2O*
4,4’,4’’-trimethoxytriphenylmethyl cation	482	0.77	0.82
4,4’-dimethoxytriphenylmethyl cation	482	–1.70	–1.24
4-methoxytriphenylmethyl cation	471	–4.36	–3.40
triphenylmethyl cation	430	–6.24	–6.63
4,4’,4’’-Trichlorotriphenylmethyl cation	460	–7.45	–7.74
9-phenyl-9-fluorenyl cation	488	–10.53	–10.82

* References from[1,3]

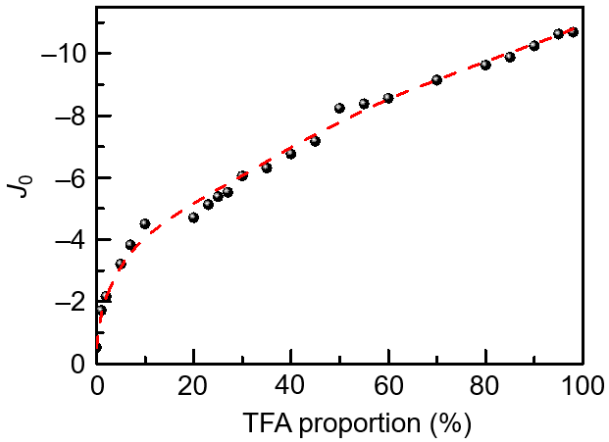

Figure S5. The TFA proportion–J_0 relationship. Data come from Table S2. The red dash line shows the eye guide for the relationship.

For the molecular wire **6**, the ratios of acetate/carbocation forms in different TFA/HAc solutions were derived from similar methods as before. The results were shown in Table S4. In combination with the J_0 values in Figure S5, the combination constants were calculated as pK_{R+} = ~–10.50, which was closely similar to the corresponding kernel.

Table S4. The ratios of acetate form and carbocation form of Compound 6.

Proportion			Carbocation (%)
HAc%	TFA%	H_2SO_4%	
40	60	0	0.4
30	70	0	1.0
20	80	0	5.8
15	85	0	13.1
10	90	0	30.9
5	95	0	51.1
2	98	0	55.8
0	94	6	100.0

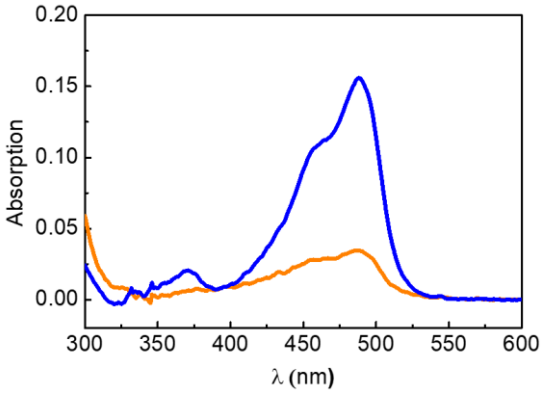

Figure S6. UV-Vis characterization of the nucleophilic competitive reaction. The solution contains 75% TFA/25% HAc and 9-phenyl-9-fluorenol at the concentration of ~4×10^{-5} mol/L. The orange/blue lines represent the conditions with/without 10 μmol/L cetyltrimethylammonium bromide, respectively. The proportion of carbocation significantly decreases when the bromide anion was added to the solution.

1.3 Kinetic Properties：

9-phenyl-9-fluorenyl cation can be generated by nanosecond laser flash photolysis and the rate constants of the combination of 9-phenyl-9-fluoerenyl cation k_c were determined in the TFA/HAc solutions with different proportions.

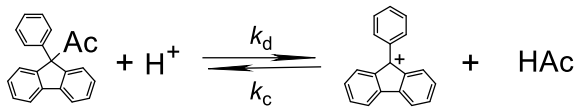

The nanosecond flash photolysis system used in this experiment had been described previously.[4,5] The dynamics of 9-phenyl-9-fluoeryl cation were measured by a nanosecond time-resolved laser flash photolysis setup of Edinburgh LP920 spectrometer (Edinburgh Instruments Ltd.), combined with a Nd:YAG laser (Surelite II, Continuum Inc.). The sample was excited by a 266 nm laser pulse (1 Hz, FWHM ~7 ns). The excitation intensity at the sample is about 1 mJ in ~1 mm spot size. The analyzing light was from a 450 W pulsed xenon lamp. The spectral range from 300 to 800 nm collected by a monochromator equipped with a photomultiplier was used to analyze the transient absorption spectra. The samples were prepared by mixing acetic acid, trifluoroacetic acid and 9-phenyl-9-fluorenol stock solution (2 mM/L). 9-phenyl-9-fluorenyl acetate was formed automatically in solution. Five samples were prepared containing 15%, 25%, 33%, 50% and 66% of TFA (by volume). The concentration for all the samples was adjusted to an absorbance of 0.3-0.5 OD at 266 nm in a 1 cm path length quartz cuvette. All experiments were carried out at room temperature.

Figure S7 shows representative time-resolved absorption spectra obtained upon 260 nm excitation (25% TFA). The maximum absorbance of photoinduced intermediates was 490 nm (since the resolution of time-resolved absorption spectra was 10 nm), which conformed to the static absorption of 9-phenyl-9-fluorenyl cation in Figure S2 (maximum absorption at 488 nm).

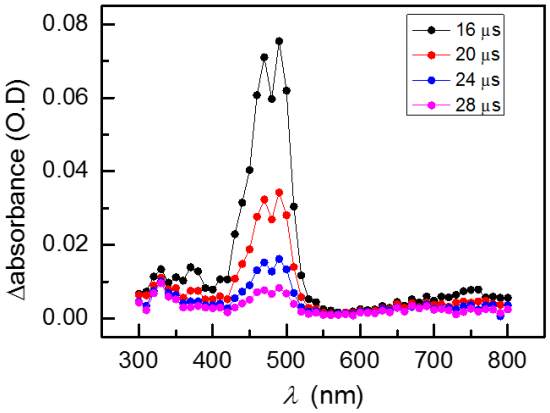

Figure S7. Time-resolved absorption spectra obtained upon 260 nm excitation of 9-phenyl-9-fluorenyl acetate in 25% TFA. Legend shows the time interval between laser pulse and acquisition of spectra.

The real-time absorbance at the maximum absorption of 9-phenyl-9-fluorenyl cation (490 nm) is shown in Figure S8. The time-absorbance plots were well-fitted in exponential decay (red lines in Figure S8), indicating that the combination of 9-phenyl-9-fluorenyl cation was a pseudo first order reaction, from which the kinetic constants k_c were fitted, respectively.

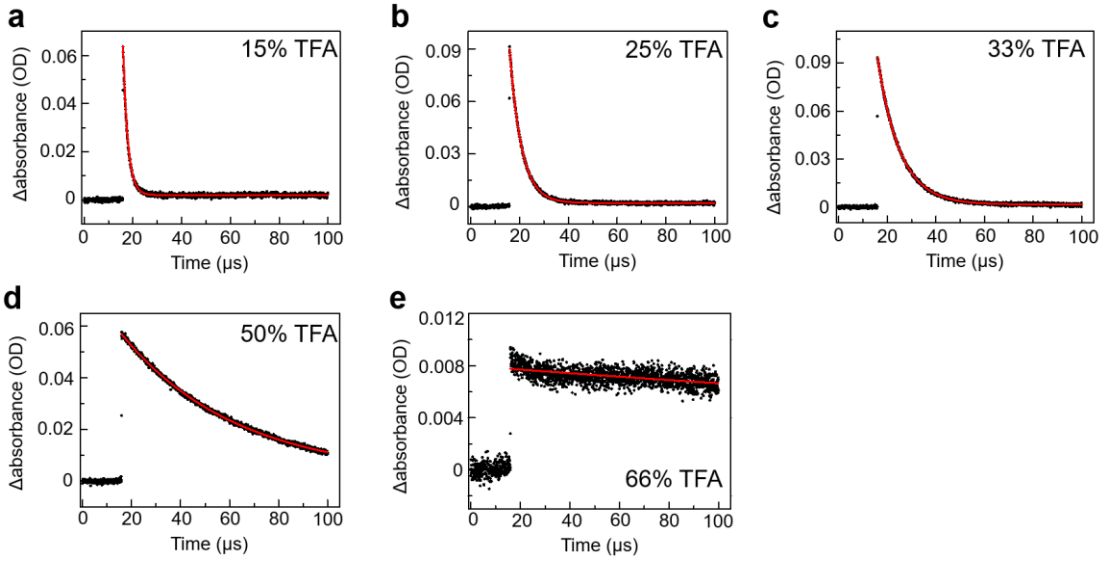

Figure S8. Real-time absorbance of 9-phenyl-9-fluorenyl cation at 490 nm in TFA/HAc solutions of different proportions. An exponential decay was fitted to the data, shown in red lines.

The disassociation rate constants k_d can be derived through k_c and the equilibrium constants (K) of the reaction:

$$K = \frac{k_d}{k_c} = \frac{[R+]}{[RAc]} \qquad \text{(Eq. 6)}$$

The equilibrium constants (K) in the TFA/HAc solutions of different proportions were derived from Equation 3, in combination with the J_0 values and the pK_{R+} value of 9-phenyl-9-fluorenyl acetate in Figure S5. For pseudo first order reactions, the mean lifetimes (τ) of acetate or carbocation are equal to the reciprocal of kinetic constants, respectively. The calculated rate constants, mean lifetimes and equilibrium constants are listed in Table S5.

Table S5. Kinetic constants, mean lifetimes of carbocation/acetate and equilibrium constants of the reaction

TFA proportion	Equilibrium constant	Kinetic constant (s^{-1})	
		k_d	k_c
15	1.23×10^{-6}	0.62 ±0.01	(5.00 ±0.08) $\times10^{5}$
25	7.08×10^{-6}	1.46 ±0.04	(2.06 ±0.05) $\times10^{5}$
33	4.68×10^{-5}	5.13 ±0.14	(1.10 ±0.03) $\times10^{5}$
50	1.78×10^{-3}	37.9 ±0.9	(2.13 ±0.05) $\times10^{4}$
66	0.0234	43.0 ±1.4	(1.83 ±0.06) $\times10^{3}$

TFA proportion	Mean lifetime (ms)	
	τ_{RAc}	τ_{R+}
15	1625 ±26	0.00200 ±0.00003
25	686 ±19	0.00485 ±0.00012
33	195 ±6	0.00909 ±0.00024
50	26.4 ±0.6	0.0470 ±0.0011
66	23.2 ±0.8	0.546 ±0.017

2. Molecular Synthesis

2.1 General:

All the solvents and reagents were purchased from commercial suppliers and used without further purification unless noted otherwise. All products were performed by flash column chromatography which was carried out with Kanto Silica Gel 60N (40-63 μm). ^{1}H NMR and ^{13}C NMR spectra were recorded at ambient temperature on a Varian 400 MHz and 100 MHz, respectively. All chemical shifts were referenced to tetramethylsilane (TMS, δ = 0.00 ppm) or relative residual peaks. Mass spectra were recorded on MALDI-TOF MS for intermediate products and HR-MS for target products.

2.2 Synthesis of 2,7-bis(4'-amino-[1,1'-biphenyl]-4-yl)-9-phenyl-9H-fluoren-9-ol (6)

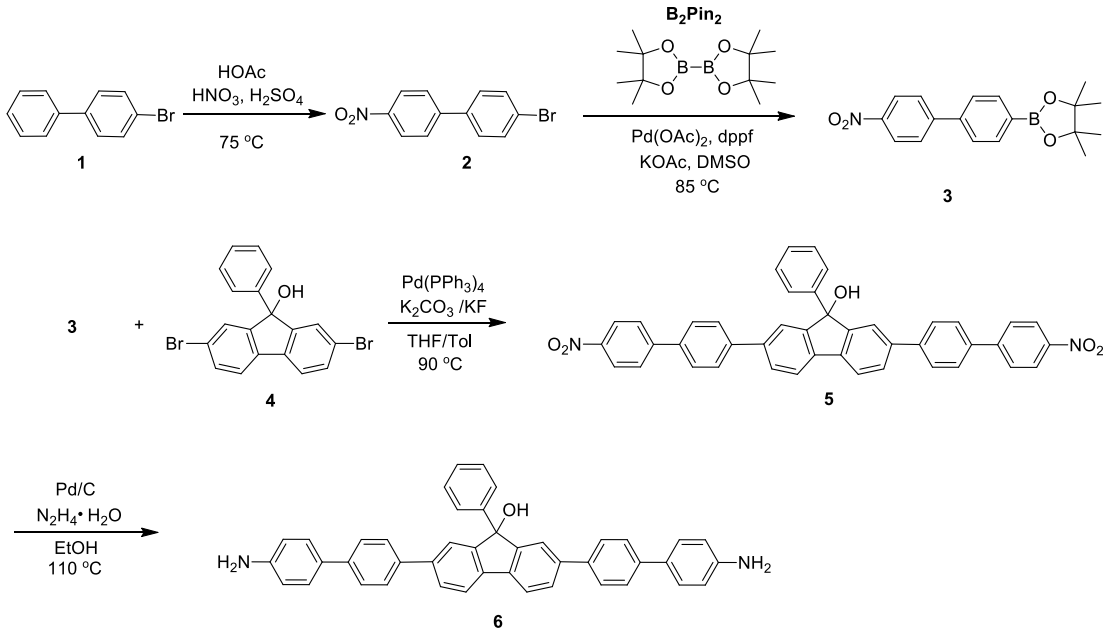

Compound 2: To a solution of **1** (2.32 g, 10 mmol) in HOAc (30 ml) at 0 °C were slowly added H_2SO_4 (2.94 g, 30 mmol) and HNO_3 (0.63 g, 10 mmol). The mixture was then slowly warmed to 75 °C, stirred for 8 h, then cooled down to room temperature. The white product (2.53 g, 91%) was collected by suction filtration, washed with water at 50 °C under vacuum. ^{1}H NMR ($CDCl_3$, 400 MHz, ppm) δ 8.29 (d, J = 8.8 Hz, 2H), 7.70 (d, J = 8.8 Hz, 2H), 7.62 (d, J = 8.5 Hz, 2H), 7.49 (d, J = 8.5 Hz, 2H). ^{13}C NMR ($CDCl_3$,100 MHz, ppm) δ 147.30, 146.34, 137.66, 132.35, 128.93, 127.65, 124.24,

123.50. GC-MS (m/z): calcd. for $C_{12}H_8BrNO_2$: 276.9 [M^+]; Found: 276.8.

Compound 3: To a solution of **2** (2.76 g, 10 mmol), B_2Pin_2 (3.04 g, 12 mmol), $Pd(OAc)_2$ (67 mg, 0.3 mmol), KOAc (2.94 g, 30 mmol) and dppf (0.332 g, 0.6mmol) in DMSO (30 ml) under a nitrogen atmosphere. The reaction mixture was stirred at 80 °C for 10 h, then cooled down to room temperature and quenched by the addition of H_2O. The aqueous portion was extracted with CH_2Cl_2. The organic layer was dried over anhydrous $MgSO_4$, filtered and the solvent was removed under reduced pressure. The crude product was purified by silica gel column chromatography (eluent, petroleum ether : CH_2Cl_2 = 20 : 1) and dried under vacuum to give **3** (2.76 g, 85%) as a white powder. ^{1}H NMR ($CDCl_3$, 400 MHz, ppm$_3$) δ 8.30 (d, J = 8.4 Hz, 2H), 7.93 (d, J = 8.2 Hz, 2H), 7.76 (d, J = 8.5 Hz, 2H), 7.63 (d, J = 8.2 Hz, 2H), 1.37 (s, 12H). ^{13}C NMR ($CDCl_3$,100 MHz, ppm) δ 147.44, 147.26, 141.26, 135.54, 127.93, 126.64, 124.10, 84.07, 24.89. GC-MS (m/z): calcd. for $C_{18}H_{20}BNO_4$: 325.1 [M^+]; Found: 325.0.

Compounds 4 and 5: Compound **4** (2,7-dibromo-9-phenyl-9*H*-fluoren-9-ol) were synthesized according to the literature procedures.[6,7] To a three-necked schlenk flask (150 mL), **4** (0.414 g, 1 mmol), **3** (0.975 g, 3 mmol) and $Pd(PPh_3)_4$ (35 mg, 0.03 mmol) were added. The flask was evacuated and back-filled with inert nitrogen gases over three times, after which degassed toluene/THF co-solvent (20 mL/20 mL) and K_2CO_3/KF (1:1) aqueous solution (2 M, 5 mL) were injected into the flask through syringe. The mixture was heated up to 90 °C and stirred for 48 h. After cooling down to room temperature, the reaction mixture was quenched by the addition of H_2O and then extracted with CH_2Cl_2. The combined organic layers were washed with water and dried over anhydrous $MgSO_4$. After filtration, the solvent was removed under reduced pressure. The crude product was purified by silica gel column chromatography (eluent, petroleum ether : CH_2Cl_2 = 1 : 5) to give compound **5** (0.51 g, 78%) as a pale yellow powder. ^{1}H NMR ($CDCl_3$, 400 MHz, ppm) δ 8.33 – 8.29 (m, 4H), 7.82 (d, J = 7.8 Hz, 2H), 7.78 – 7.75 (m, 4H), 7.74 – 7.66 (m, 10H), 7.64 (d, J = 1.3 Hz, 2H), 7.53 – 7.47

(m, 2H), 7.30 (tdd, J = 6.0, 3.9, 2.3 Hz, 3H), 2.60 (s, 1H). ^{13}C NMR ($CDCl_3$,100 MHz, ppm) δ 151.70, 147.13, 146.92, 142.83, 141.25, 140.56, 138.83, 137.70, 128.44, 128.21, 127.77, 127.71, 127.58, 127.49, 125.46, 124.18, 123.50, 120.77, 83.69. MALDI-TOF-MS (m/z): calcd. for $C_{43}H_{28}N_2O_5$: 652.20 [M^+]; Found: 651.16.

Compound 6: To a three-necked schlenk flask (50 mL) were added **5** (0.652 g, 1 mmol) and Pd/C (0.318 g, 3 mmol). The flask was evacuated and back-filled with inert nitrogen gases over three times, after which $N_2H_4 \cdot H_2O$ (0.15 g, 3 mmol) and EtOH (20 ml) were injected into the flask through syringe. The mixture was heated up to 110 ℃ and stirred for 36 h. After cooling down to the room temperature, Pd/C was removed by suction filtration. The filtrate was extracted three times with CH_2Cl_2 and the organic layer was dried over anhydrous $MgSO_4$. After filtration, the solvent was removed under reduced pressure. The crude product was purified by silica gel column chromatography (eluent, petroleum ether : ethyl acetate = 1 : 1) to give compound **6** (0.36 g, 61%) as a pale yellow powder. ^{1}H NMR ($CDCl_3$, 400 MHz, ppm) δ 7.77 (d, J = 7.9 Hz, 2H), 7.68 (dd, J = 7.9, 1.7 Hz, 2H), 7.64 – 7.61 (m, 4H), 7.58 (d, J = 8.6 Hz, 3H), 7.50 (dd, J = 8.9, 7.4 Hz, 2H), 7.47 – 7.41 (m, 3H), 7.33 – 7.26 (m, 4H), 7.26 – 7.21 (m, 4H), 6.80 – 6.74 (m, 3H), 3.75 (s, 4H), 2.59 (s, 1H). ^{13}C NMR (d_6-DMSO, 100 MHz, ppm) δ 152.93, 149.04, 140.21, 140.05, 138.50, 137.49, 128.61, 127.51, 127.29, 127.22, 127.08, 126.22, 125.71, 122.82, 121.29, 114.72, 83.10. MALDI-TOF-MS (m/z): calcd. for $C_{43}H_{32}N_2O$: 592.25 [M^+]; Found: 591.04. HR-MS (ESI+, m/z): calcd. For $C_{43}H_{32}N_2O$: 593.2587 [$M+H^+$]; Found: 593.2599.

2.3 Synthesis of [1,1':4',1'':4'',1''':4''',1'''':4'''',1''''':4''''',1'''''-sexiphenyl]-4,4'''''-diamine

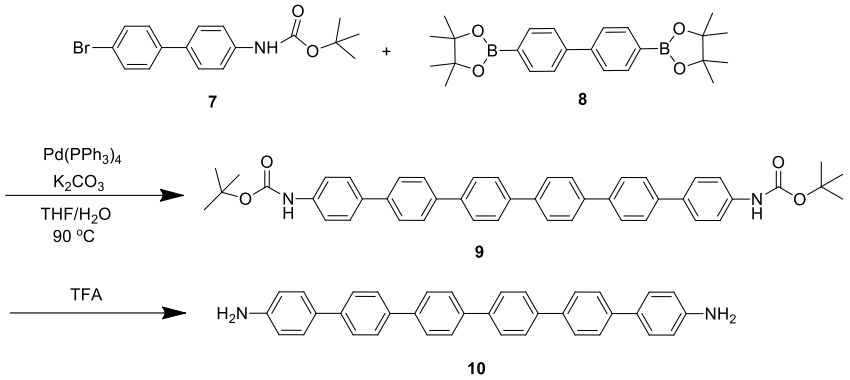

To a three-necked schlenk flask (150 mL) were added **7** (1.04 g, 3 mmol), **8** (0.41 g, 1 mmol), K_2CO_3 (1.80 g, 13.0 mmol), and $Pd(PPh_3)_4$ (58 mg, 0.05 mmol). The flask was evacuated and back-filled with inert argon gases over three times, after which a degassed THF/H_2O co-solvent (15 mL/7 mL) were injected into the flask through syringe. The mixture was heated up to 90 °C and stirred for 14 h. After cooling down to room temperature, the reaction mixture was poured into water, and then extracted with CH_2Cl_2. The organic layer was dried over anhydrous $MgSO_4$ and filtered off from an insoluble fraction. The solvent was removed under reduced pressure. Then the crude product was purified by silica gel column chromatography (eluent, petroleum ether : ethyl acetate = 9 : 1) to give compound **9** as a light yellow powder. This solid was then dissolved in a mixture of CH_2Cl_2 (3 mL) and TFA (3 mL) and stirred for 2 h at room temperature. The solvent was removed under vacuum to give the target compound **10** (0.37 g, 75%) as a light yellow powder. ^{1}H NMR (d_6-DMSO, 400 MHz, ppm) δ 7.99 – 7.60 (m, 16H), 7.47 (d, J = 7.4 Hz, 4H), 6.67 (d, J = 6.7 Hz, 4H), 5.28 (s, 4H). HR-MS (MALDI-TOF, m/z): calcd. For $C_{36}H_{28}N_2$: 488.2252 [M^+]; Found: 488.2265.

3. Device Characterization and Analysis

3.1 Device Fabrication and Characterization

The devices with graphene point contact arrays were fabricated by a dash-line lithographic (DLL) method described elsewhere before in detail.[8] In brief, single-layered graphene was synthesized via a chemical vapor deposition (CVD) process on copper foils. After graphene films were transferred to SiO_2/Si wafers, metal electrodes were subsequently patterned by using photolithography. The nanogapped graphene point contact arrays with carboxylic acid groups on each side were fabricated by the DLL method. In order to prevent any direct contact and leakage between the HAc/TFA solution and metal electrodes during electrical measurements, a 50 nm-thick silicon oxide layer was deposited by e-beam thermal evaporation after resistance thermal deposition of patterned metallic electrodes (8/60 nm, Cr/Au). After the device fabrication, the molecular wire was dissolved into anhydrous pyridine at the concentration of 10^{-4} mol/L. The freshly-prepared devices and 1-ethyl-3-(3-dimethylaminopropyl) carbodiimide hydrochloride (EDCI), as a dehydrating/carboxyl activating agent, were added to the pyridine solution under the protection of argon. After reaction for 72 h, the devices were taken out from the solution, washed with acetone and isopropanol alternatively, and then dried under a nitrogen stream. After molecular connection, the devices were electrically characterized with an Agilent 4155C semiconductor characterization system (Figure S9a). We found that the current decreased to zero after precise oxygen plasma etching and recovered to some extent after molecular immobilization, indicating the success of the device fabrication. After *I–V* characterization, microscopic polydimethylsiloxane (PDMS) liquid storage pools were immobilized on the central area of the devices (Figure S9b). High temporal resolution *I–t* measurements were carried out with an HF2LI Lock-In Amplifier and a DL 1211 Current Amplifier. The devices were firstly measured in the air. Then, 15 μL HAc was introduced to the PDMS pool with a microscopic syringe. Extra 5 μL, 15 μL and 45 μL TFA was added to the pool to form the TFA/HAc solutions with the proportions of 25%/75%, 50%/50% and 75%/25%, respectively. Finally, a 20 μL Br^-

/HAc/TFA stock solution, which consisted of a 75%/25% TFA/HAc solution with ~40 μmol/L hexadecyltrimethyl ammonium bromide, was introduced to the pool to provide different nucleophiles (Br^- and Ac^-). A minicap was applied to the pool to prevent the solution volatilization. After each solution introduction, real-time conductance measurements were carried out for at least 1 min. The bias voltages were set at 300 mV and the sampling rate was 57.6 kSa/s for all measurements.

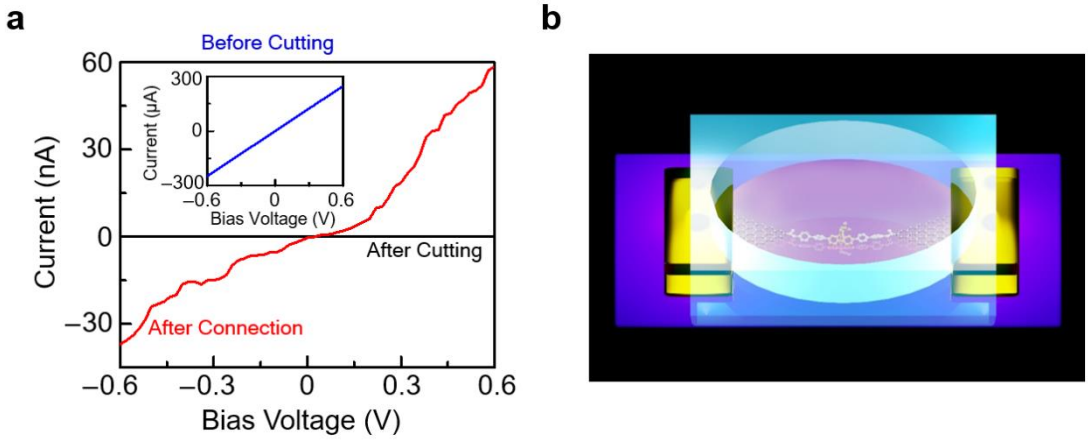

Figure S9. Device characterization. (a) Representative *I–V* curves for the graphene sheet before dash-line lithography (blue), graphene point electrodes before molecular connection (black) and single-molecule junction after molecular connection (red). (b) Schematic of a device with a liquid reservoir formed from PDMS.

3.2 Single-molecule Connection Analysis

The ratio of single-junction devices to the overall reconnected devices is evaluated by statistics based on a binomial distribution reported before.[8] Particularly, the probability of the connected devices with *n*-rejoined junctions (G_n) can be calculated from a binomial distribution in Eq. 7, where *m* is the number of graphene point contact pairs (210 in this case), *p* is the connection success rate for each pair.

$$G_n = \frac{m!}{n!(m-n)!}p^n(1-p)^{m-n} \qquad n = 0, 1, 2 \cdots, m \qquad \text{(Eq. 7)}$$

$$Y_{\text{connection}} = 1 - G_0 = 1 - \frac{m!}{0!(m-0)!}p^0(1-p)^m \qquad \text{(Eq. 8)}$$

The optimized connection yield ($Y_{\text{connection}}$) equals to 1 – G_0, where G_0 is the probability of devices without any connection (Eq. 8). According to the statistic results in the main

text, the optimized connection yield ($Y_{connection}$) was ~15%. In combination with Eqs. 7-8, the probability of the connected device with a single junction is ~92%. That means, in most cases, charge transport in these devices mainly exists in a single-molecule junction.

4. Characterization of Control Devices:

4.1 Graphene Sheets

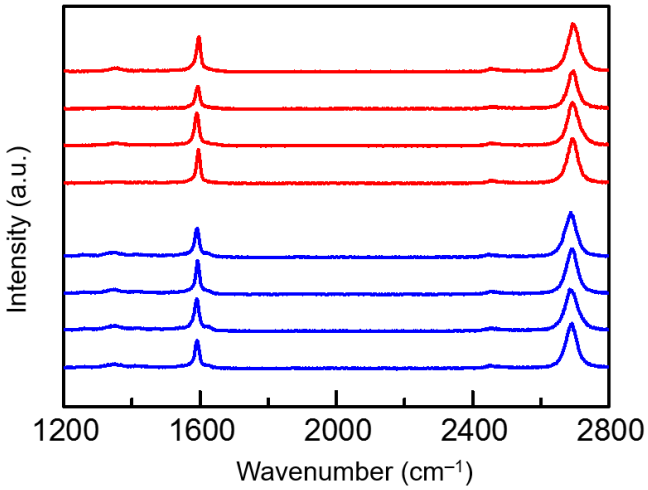

Figure S10. Raman spectra of four representative single-layer graphene samples before (blue line) and after (red) immersion into a TFA/HAc (75%/25%, vol/vol) solution for 1 h. Raman spectra show that TFA/HAc solutions do not obviously affect the properties of graphene.

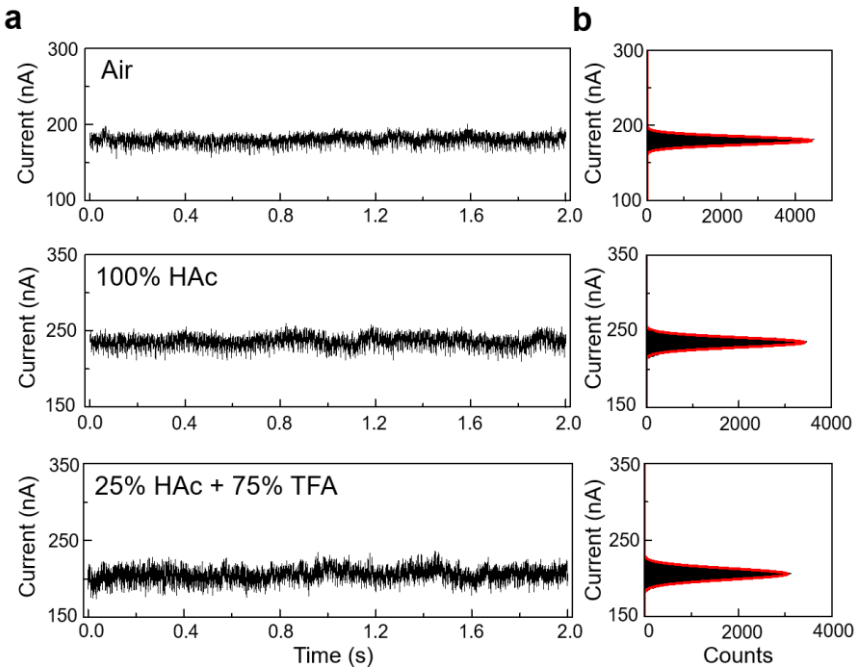

Figure S11. Control experiments by using a 40μm wide graphene device at 3 mV. (a) *I–t* curves of a control device in the air, pure acetic acid and TFA/HAc (75%/25%, vol/vol) solutions. The current was in the same magnitude as the device in the main text. (b) The corresponding histograms of (a**)**, showing a gauss-shaped current distribution.

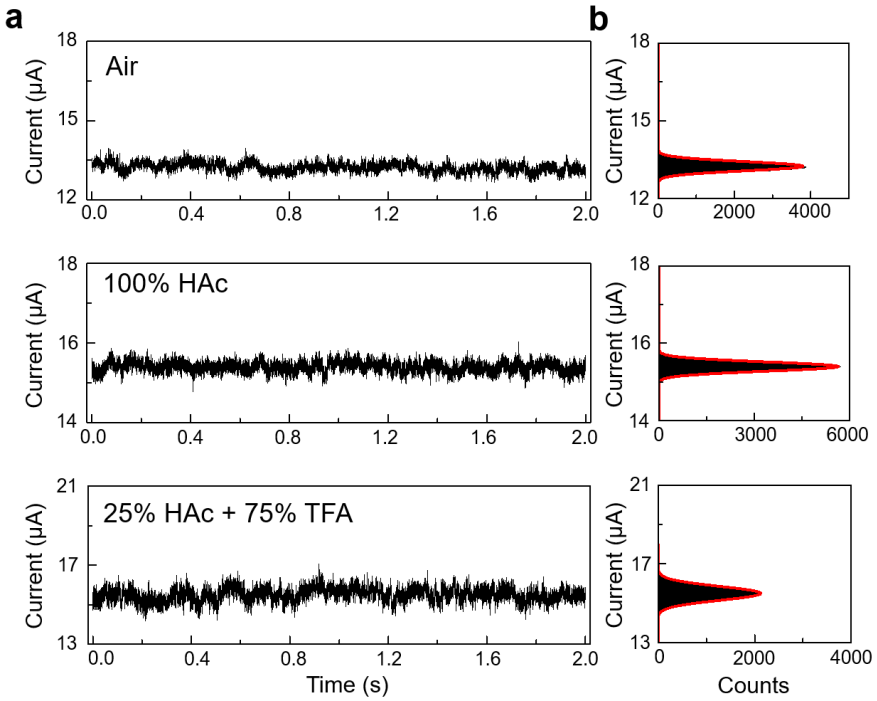

Figure S12. Control experiments by using a 40μm wide graphene ribbon at 300 mV. (a) *I–t* curves of a control device in the air, pure acetic acid and TFA/HAc (75%/25%, vol/vol) solutions. The applied bias voltage is the same as the device in the main text. (b) The corresponding histograms of (a), showing a gauss-shaped current distribution.

4.2 Partially-Cleaved Graphene Nanoconstriction

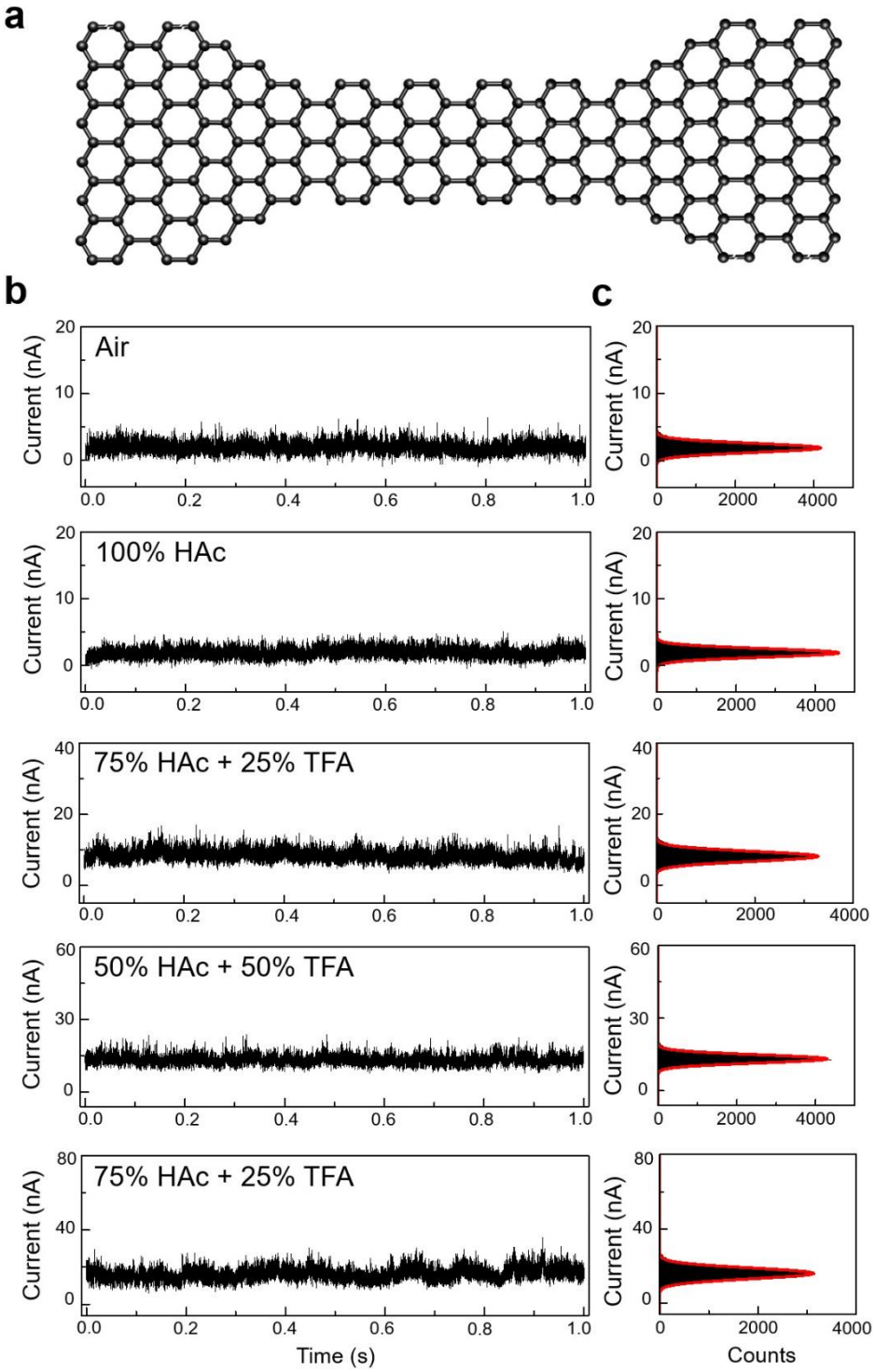

Figure S13. Control experiments by using a partially-cleaved graphene nanoconstriction at 300 mV. (a) Schematic of a partially-cut graphene nanoconstriction. (b) *I–t* curves of a control device in the air, pure acetic acid and TFA/HAc (25%/75%, 50%/50%, 75%/25%, vol/vol) solutions. The current was in the same magnitude as the device in the main text. (c) The corresponding histograms of (b), showing a gauss-shaped current distribution.

4.3 Acid-Inert GMG-SMJs

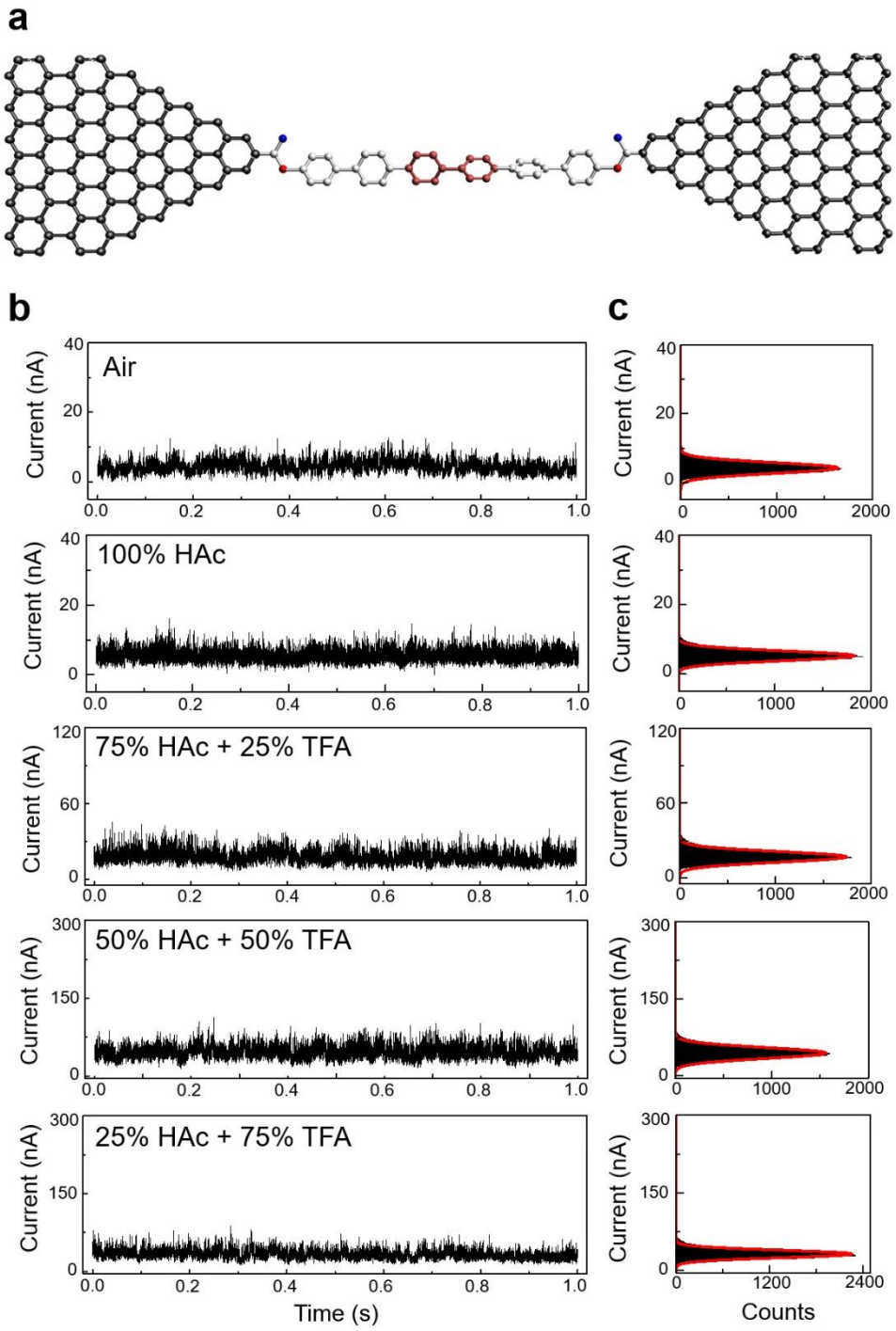

Figure S14. Control experiments by using an acid-inert hexaphenyl connected SMJ device at 300 mV. (a) Schematic of a hexaphenyl connected SMJ. Compared with the molecule applied in the main text, the core of the molecular wire was replaced by a non-function biphenyl group (shown in red). (b) *I–t* curves of the control device in the air, pure acetic acid and TFA/HAc (25%/75%, 50%/50%, 75%/25%, vol/vol) solutions. The current was in the same magnitude as the device in the main text. (c) The corresponding histograms of (b), showing a gauss-shaped current distribution.

5. Theoretical Analysis and Physical Properties

5.1 Electronic Structures

The structural relaxation of the isolated molecules and two-probe transport junctions were carried out by the projector augmented wave (PAW) method as implemented in the Vienna Ab initio simulation package (VASP).[9] The exchange-correlation was treated at the Perdew-Burke-Ernzerhof generalized gradient approximation (PBE-GGA) level.[10,11] The plane wave basis was set to a kinetic energy cutoff of 400 eV. The relaxation was deemed completed when the residual force on each atom was less than 0.01 eV/Å. The electronic structures of the relaxed isolated molecules were calculated by density functional theory (DFT) within the Gaussian package.[12] The B3LYP hybrid functional and the 6-31G basis set were taken in the Gaussian calculation. The charge transport properties of the two-probe structures were obtained by carrying out density functional theory (DFT) within the nonequilibrium Green's function (NEGF) formalism, as implemented in the quantum transport package Nanodcal.[13,14] Double-zeta polarized atomic orbital basis set was used in the NEGF-DFT calculation, and exchange-correlation is treated at the PBE-GGA level. The cutoff energy for the real-space grid was set at 1360 eV. The NEGF-DFT self-consistent calculations were deemed converged when every element of the Hamiltonian matrix and the density matrix were converged to less than 10^{-5} a.u. Afterward the transmission spectra and scattering states were calculated by the Green's function and scattering matrix methods (Figure 3c and Figure S16).

In the calculated frontier molecular orbitals, the carbocation form shows totally different density of states (DOS) distribution, compared with the acetate/bromide forms (Figure 3b in the main text). (i) DOS exists in the side phenyl group of the carbocation form, which results in a more conjugated structure in the 9-phenyl-9-fluorenyl functional core. Such a conjugated structure obviously decreases the frontier molecular orbital (FMO) gaps of the carbocation form, which reflects in the calculated results and measured optical data. (ii) The calculated DOS is delocalized in the main chain of the acetate/bromide form, while localized in the core of the carbocation form. This means

that the modified biphenyl chains affect more strongly the property of the acetate/bromide form than that of the carbocation form. These results are also reflected in the spectroscopy measurements (Figure S15): For the acetate form, the absorption moved from 277 nm to 334 nm, but for the carbocation form the absorption only slightly moved from 493 nm to 500 nm after the modification by the biphenyl groups.

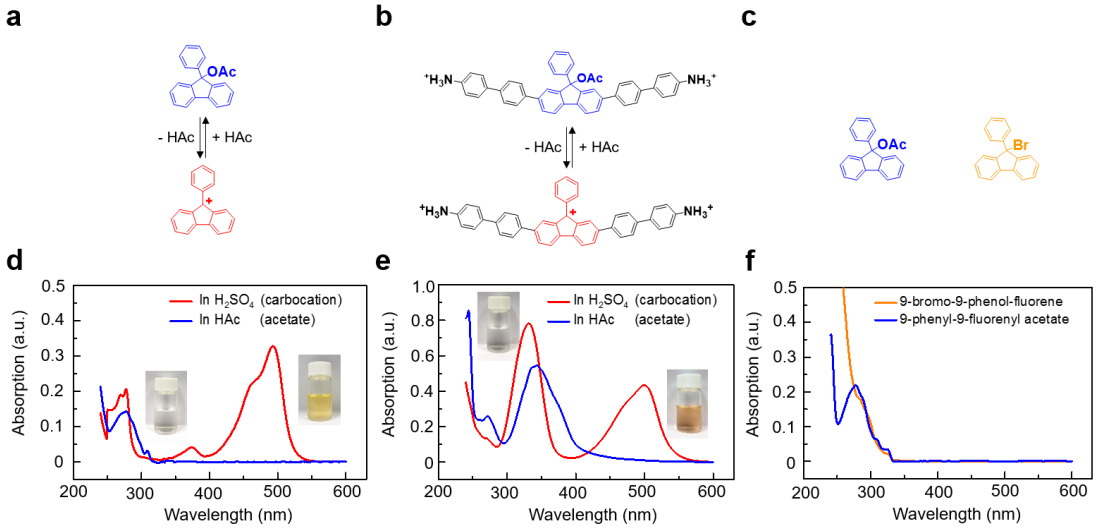

Figure S15. UV-Vis measurements. (a,b) Schematic of the transitions between the acetate form (blue) and the carbocation form (red) for 9-phenyl-9-fluorenyl acetate (a) and the molecular wire (b). (c) The structures of 9-phenyl-9-fluorenyl acetate (blue) and 9-phenyl-9-bromo-fluorene (orange). (d,e) UV-Vis absorption spectra of the 9-phenyl-9-fluorenyl acetate (d) and the molecular wire (e) at the concentration of ~2×10^{-5} mol/L in the solution of sulfuric acid (red) and acetic acid (blue), showing the complete transition of carbocation forms and acetate forms. (f) UV-Vis absorption spectra of 9-phenyl-9-fluorenyl acetate and 9-phenyl-9-bromo-fluorene at the concentration of ~2×10^{-5} mol/L in the solution of dichloromethane.

5.2 Transport Properties

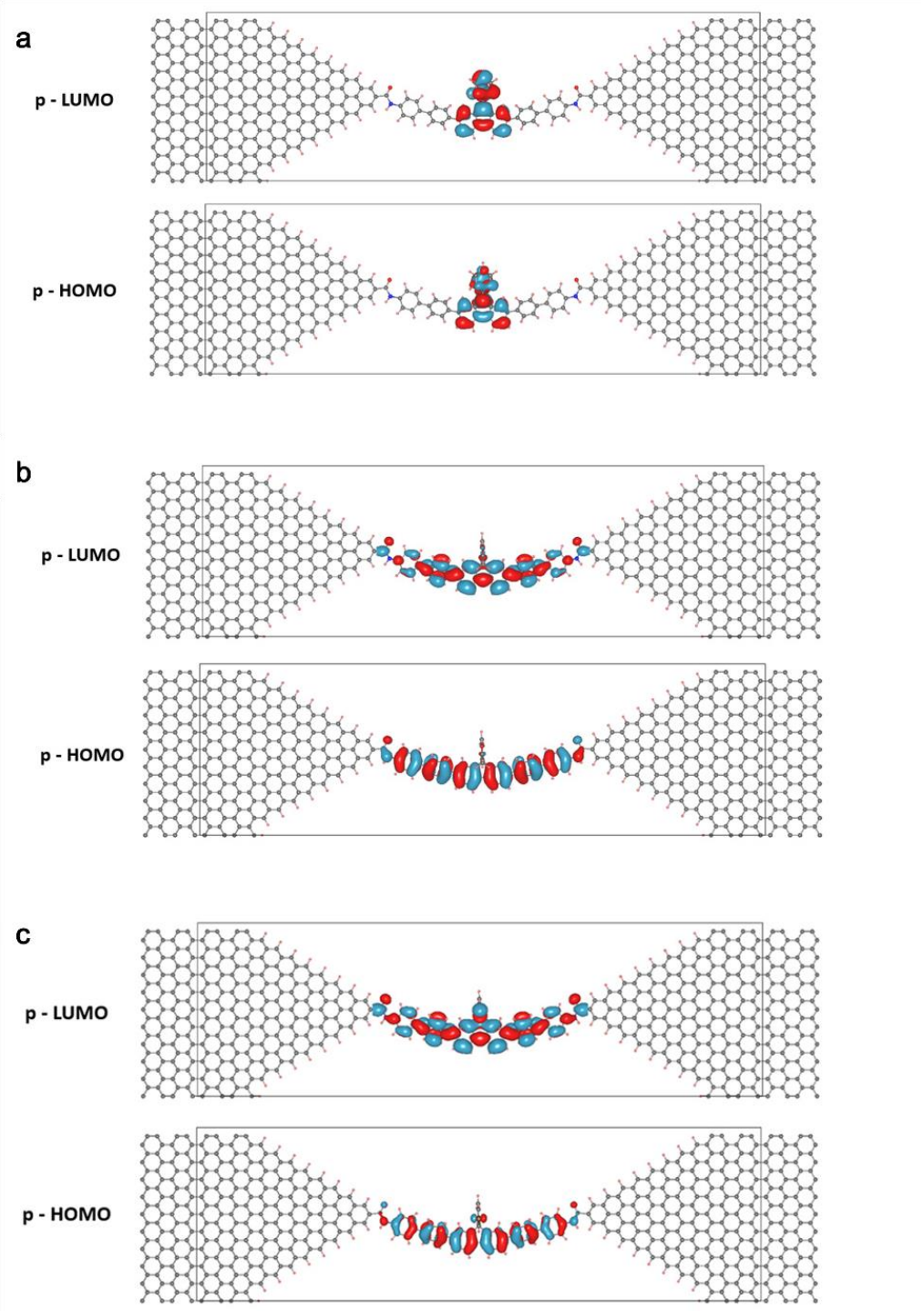

Figure S16. The scattering states of the p-HOMOs and p-LUMOs of carbocation form (a), acetate form (b) and bromide form (c). For a clear expression only the scattering states of the central molecule are shown.

6. Dynamic Analysis

Thermodynamics & kinetics parameters derived from GMG-SMJs were calculated as follows: the *I*–*t* trajectories were idealised into a two-state interconversion by a QUB software and the distributions of their lifetimes were analysed independently (Figure S17). The distributions were fit in a single exponential decay function: $P(\tau) = k\exp(-k\tau)$, where $P(\tau)$ represents the probability density, τ is the dwell time and k is the rate constant. The activation energies E were derived from the Eyring equation: $E = RT\ln(\frac{k_B T}{hk})$, where R = 8.314 J/(mol·K), T is the temperature, k_B is the Boltzmann constant, and h is the plank constant. The equilibrium constants (K) were derived from Eq. 6 in the Supporting Information. The combination constants (pK_{R+}) were normalized by TFA proportion–J_0 relationship from Figure S5 at different TFA/HAc proportions: $pK_{R+} = J_0 + pK$.

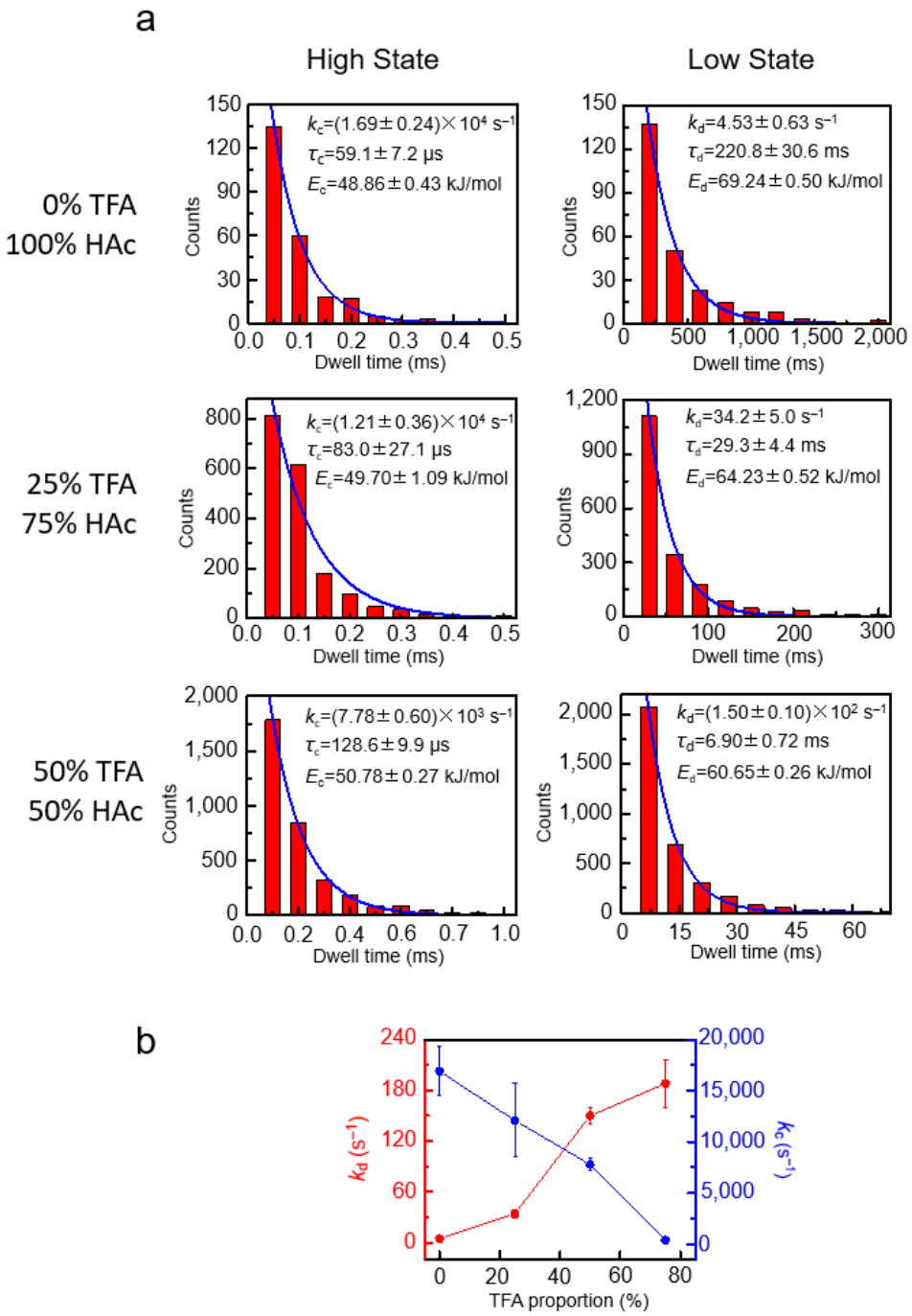

Figure S17. Kinetic analyses. (a) The frequency distribution diagrams derived from the device in Figure 2 (red columns). The distributions were well fitted in a single-exponential distribution (blue lines), from which the reaction kinetic constants (k), mean lifetimes (τ) and activation energies (E) were derived according to the equations in Section 6. (b) Plots of the dissociation/combination rate constants (k_d and k_c) at different HAc/TFA solutions.

Table S6. Summary of kinetic/thermodynamic properties derived from the device in Figure 2.

		TFA%			
		0	25	50	75
High State	k_c (s^{-1})	(1.69±0.24)×10^4	(1.21±0.36)×10^4	(7.78±0.60)×10^3	(3.94±0.29)×10^2
	τ_{high} (μs)	59.1 ± 7.2	83.0 ± 27.1	128.6 ± 9.9	2540 ± 200
	E_c (kJ·mol^{-1})	48.86 ± 0.43	49.70 ± 1.09	50.78 ± 0.27	58.18 ± 0.27
Low State	k_d (s^{-1})	4.53 ± 0.63	34.2 ± 5.0	(1.50±0.10)×10^2	(1.88±0.28)×10^2
	τ_{low} (ms)	220.8 ± 30.6	29.3 ± 4.4	6.90 ± 0.72	5.32 ± 0.79
	E_d (kJ·mol^{-1})	69.24 ± 0.50	64.23 ± 0.52	60.65 ± 0.26	60.01 ± 0.52
p*K*		3.57 ± 0.11	2.55 ± 0.21	1.73 ± 0.06	0.32 ± 0.20
pK_{R+}		–4.10 ± 0.11	–8.11 ± 0.21	–9.46 ± 0.06	–9.72 ± 0.20

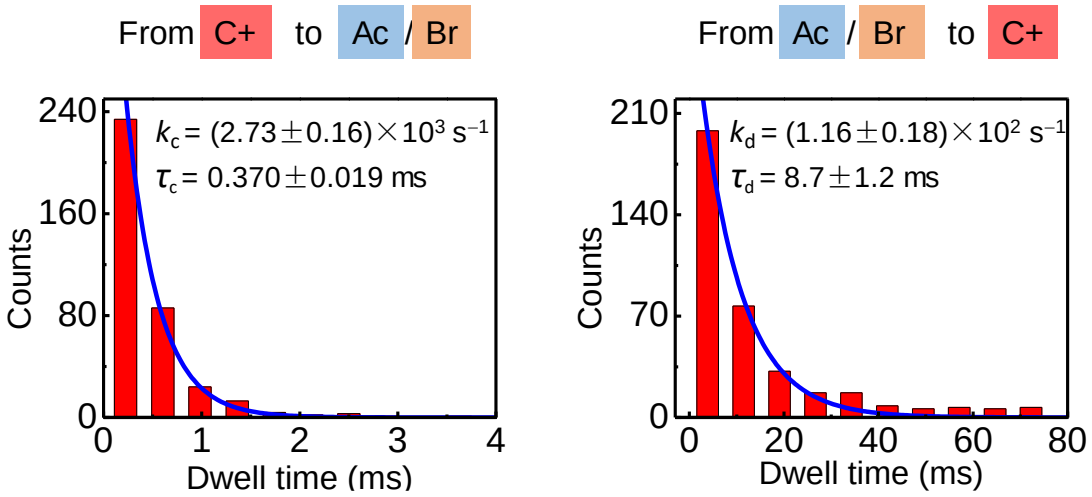

Figure S18. Kinetic analysis. The diagrams of the frequency distributions were derived from the device in Figure 5 (red columns). The distributions were well fitted in a single-exponential distribution (blue lines), from which the reaction kinetic constants (k) and mean lifetimes (τ) were derived according to the equations in Section 6.

7. Additional Experimental Results

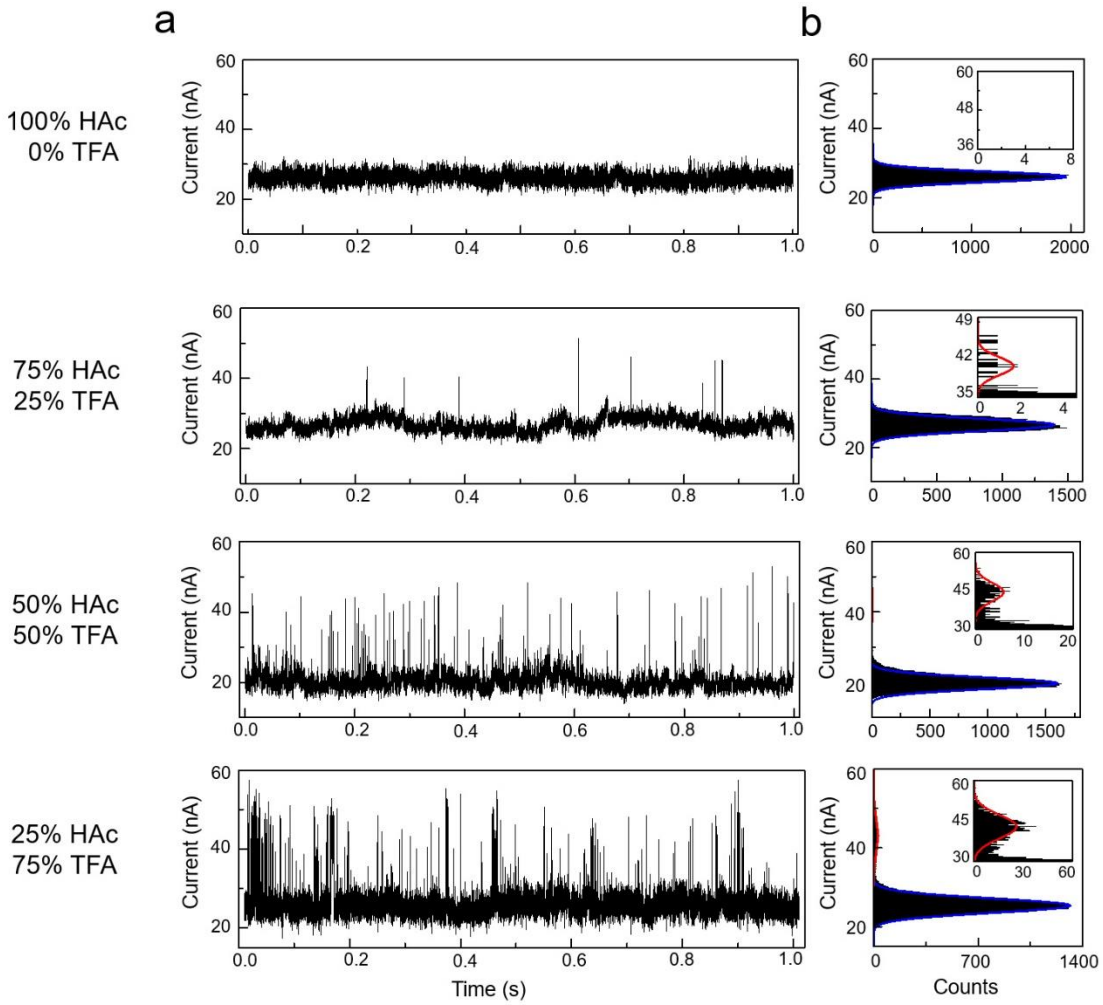

Figure S19. Another set of real-time measurements from a different GMG-SMJ device. The measurements were carried out in the same condition as Figure 2, revealing similar results. (a) *I–t* curves of the device in the pure acetic acid and TFA/HAc (25%/75%, 50%/50%, 75%/25%, vol/vol) solutions. (b) The corresponding histograms of (a), showing a gauss-shaped current distribution.

Table S7. Kinetic/thermodynamic properties derived from the device in Figure S19.

		TFA%			
		0	25	50	75
High State	k_c (s^{-1})	–	$(1.69 \pm 0.43) \times 10^4$	$(1.48 \pm 0.32) \times 10^4$	$(2.40 \pm 0.67) \times 10^3$
	τ_{high} (μs)	–	59.0 ± 20.2	67.4 ± 11.9	417 ± 92
	E_c (kJ mol^{-1})	–	48.86 ± 0.73	49.19 ± 0.48	53.70 ± 0.62
Low State	k_d (s^{-1})	–	14.2 ± 4.2	70.2 ± 13.2	439 ± 116
	τ_{low} (ms)	–	70.6 ± 30.6	13.9 ± 2.8	2.28 ± 0.46
	E_d (kJ mol^{-1})	–	66.41 ± 0.86	62.45 ± 0.52	57.91 ± 0.56
	p*K*	–	3.08 ± 0.23	2.32 ± 0.12	0.74 ± 0.21
	pK_{R+}	–	–8.65 ± 0.23	–10.05 ± 0.12	–10.13 ± 0.21

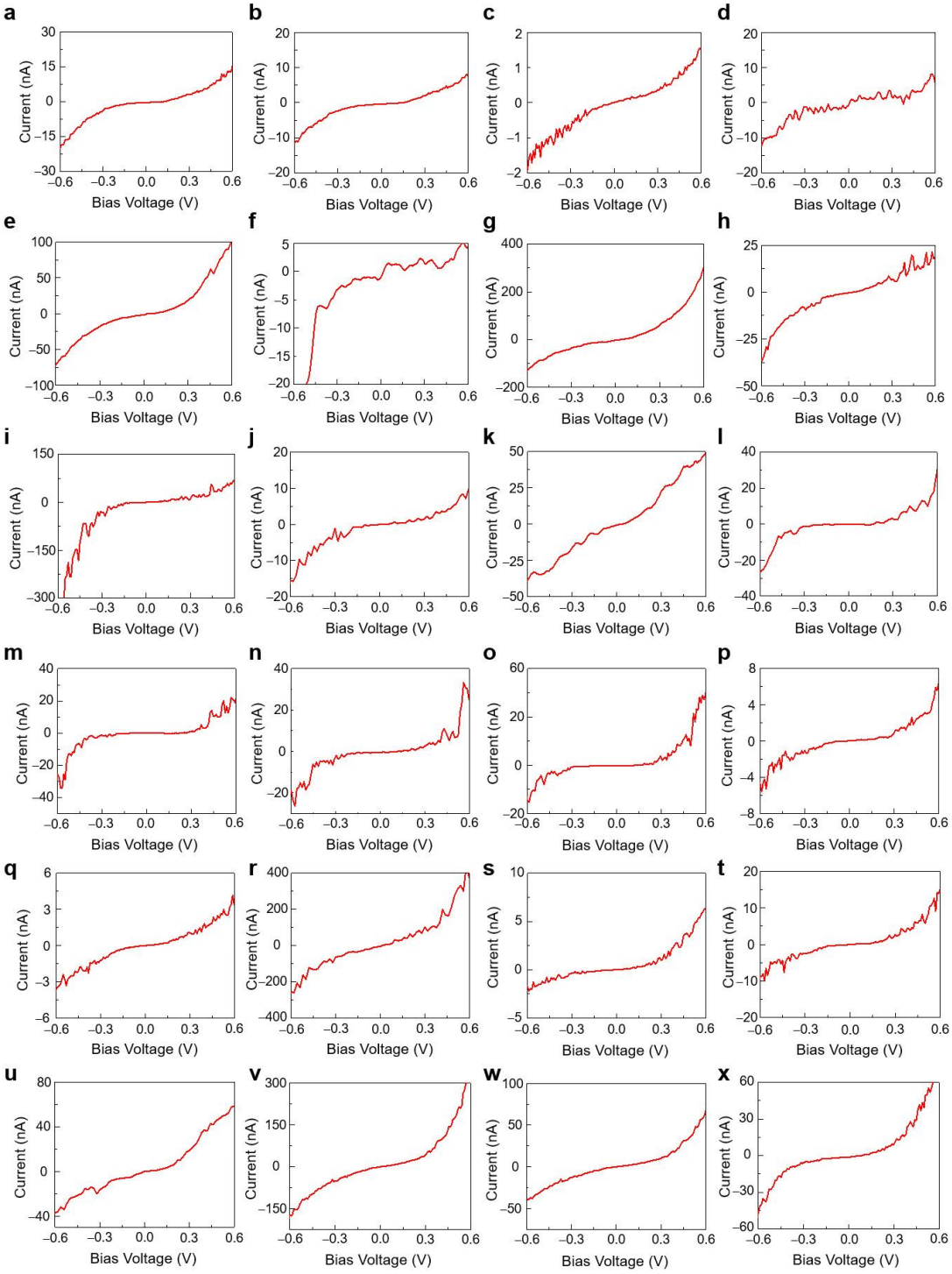

Figure S20. *I–V* curves of additional 24 GMG-SMJ devices measured in the air.

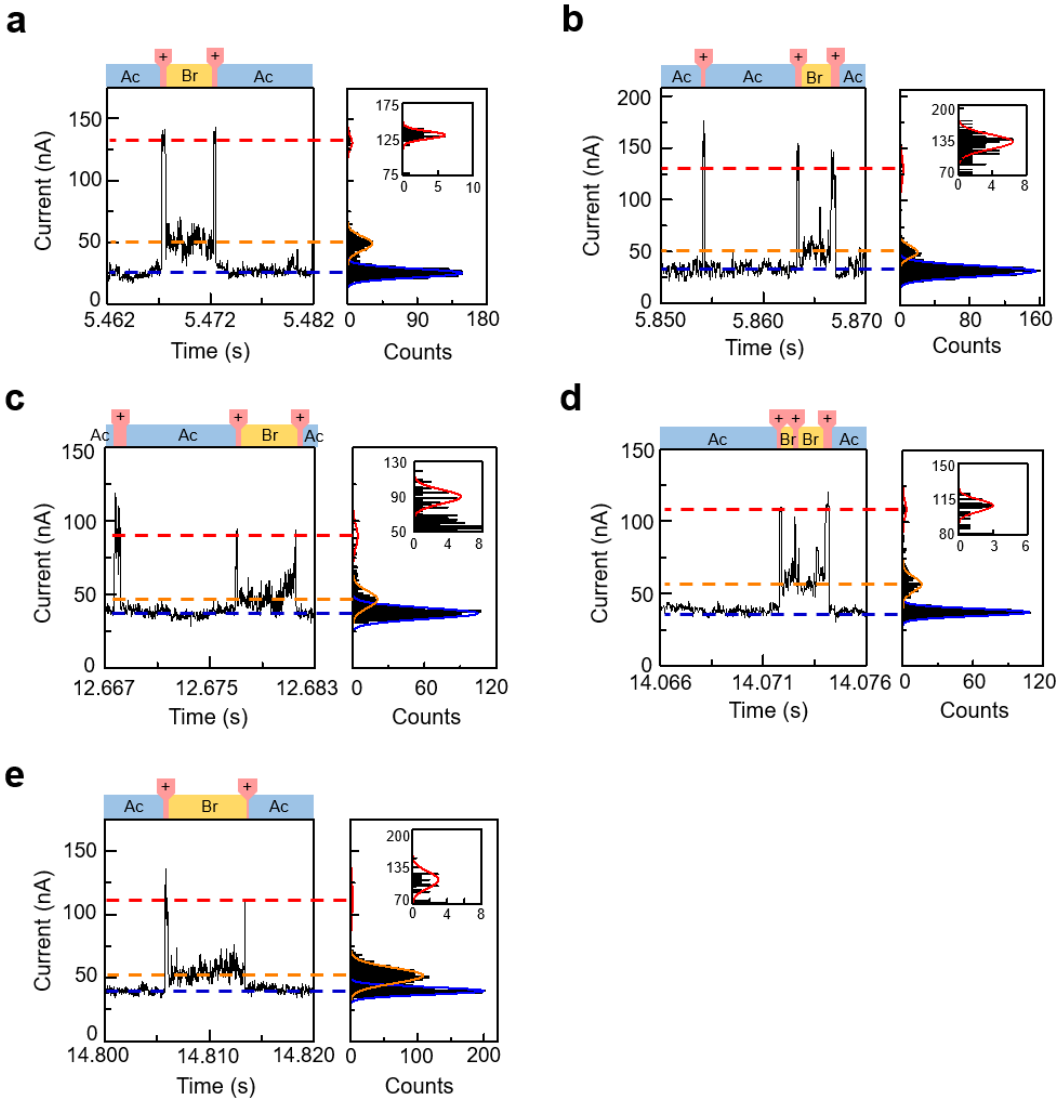

Figure S21. Additional *I–t* trajectory fragments of a 9-phenyl-9-fluorenyl functionalized SMJ submerged into a Br^-/HAc/TFA ternary solution (in the same condition as Figure 5). Ac, Br and + represent the acetate form, the bromide form and the carbocation form, respectively.

8. References:

(1) Deno, N. C.; Berkheimer, H. E.; Evans, W. L.; Peterson, H. J. *J. Am. Chem. Soc.* **1959**, *81*, 2344–2347.

(2) Gold, V.; Hawes, B. W. V. *J. Chem. Soc.* **1951**, *39*, 2102–2111.

(3) Toone, T. W.; Lee-Ruff, E.; Hopkinson, A. C. *Can. J. Chem.* **1975**, *53*, 1635–1641.

(4) Yang, C.; Su, H.; Sun, X.; George, M. W. *J. Chem. Phys.* **2012**, *136*, 204507.

(5) Wang, X.; Hu, J.; Li, Y.; Jie, J.; Xia, A. *J. Phys. Chem. C* **2016**, *120*, 598–605.

(6) Xie, L. H.; Hou, X. Y.; Hua, Y. R.; Tang, C.; Liu, F.; Fan, Q. L.; Huang, W. *Org. Lett.* **2006**, *8*, 3701–3704.

(7) Wong, K. T.; Wang, Z. J.; Chien, Y. Y.; Wang, C. L. *Org. Lett*. **2001**, *3*, 2285–2288.

(8) Cao, Y.; Dong, S.; Liu, S.; He, L.; Gan, L.; Yu, X.; Steigerwald, M. L.; Wu, X.; Liu, Z.; Guo, X. *Angew. Chem. Int. Ed.* **2012**, *51*, 12228–12232.

(9) Kresse, G.; Furthmüller, *J. Phys. Rev. B* **1996**, *54*, 11169–11186.

(10) Perdew, J. P.; Burke, K.; Ernzerhof, M. *Phys. Rev. Lett.* **1996**, *77*, 3865–3868.

(11) Blöchl, P. E. *Phys. Rev. B* **1994**, *50*, 17953–17979.

(12) Frisch M. J. **2004**, revision C.02; Gaussian, Inc.: Wallingford, CT.

(13) Taylor, J.; Guo, H.; Wang, J. *Phys. Rev. B* **2001**, *63*, 245401.

(14) Li, Z.; Smeu, M.; Afsari, S.; Xing, Y.; Ratner, M. A.; Borguet, E. *Angew. Chem. Int. Ed.* **2014**, *53*, 1098–1102.